The van der Waals epitaxy of Bi_2Se_3 on the vicinal Si(111) surface: an approach for preparing high-quality thin films of a topological insulator

2010 New J. Phys. 12 103038

(http://iopscience.iop.org/1367-2630/12/10/103038)

New Journal of Physics
The open-access journal for physics

The van der Waals epitaxy of Bi_2Se_3 on the vicinal Si(111) surface: an approach for preparing high-quality thin films of a topological insulator

H D Li[1,2], Z Y Wang[1], X Kan[1], X Guo[1], H T He[3], Z Wang[3], J N Wang[3], T L Wong[3], N Wang[3] and M H Xie[1,4]

[1] Physics Department, The University of Hong Kong, Pokfulam Road, Hong Kong, People's Republic of China
[2] Department of Physics, Beijing Jiaotong University, Beijing 100044, People's Republic of China
[3] Physics Department, Hong Kong University of Science and Technology, Clear Water Bay, Kowloon, Hong Kong, People's Republic of China
E-mail: mhxie@hkusua.hku.hk

New Journal of Physics **12** (2010) 103038 (11pp)
Received 10 June 2010
Published 26 October 2010
Online at http://www.njp.org/
doi:10.1088/1367-2630/12/10/103038

Abstract. The epitaxial growth of thin films of the topological insulator Bi_2Se_3 on nominally flat and vicinal Si(111) substrates was studied. In order to achieve a planar growth front and better quality epifilms, a two-step growth method was adopted for the van der Waals epitaxy of Bi_2Se_3 to proceed. By using vicinal Si(111) substrate surfaces, the in-plane growth rate anisotropy of Bi_2Se_3 was exploited in order to achieve single crystalline Bi_2Se_3 epifilms, in which threading defects and twins are effectively suppressed. The optimization of the growth parameters has resulted in the vicinal Bi_2Se_3 films showing a carrier mobility of $\sim 2000\,cm^2\,V^{-1}\,s^{-1}$ and a background doping of $\sim 3 \times 10^{18}\,cm^{-3}$ of the as-grown layers. Such samples not only show a relatively high magnetoresistance but also show a linear dependence on the magnetic field.

[4] Author to whom any correspondence should be addressed.

Contents

1. Introduction

Bi_2Q_3 (Q = Se, Te) compounds are classical thermoelectric materials with a high figure of merit ZT (e.g. $ZT \approx 1$ for Bi_2Te_3) [1]–[3]. Recently, a significant resurgence of interest in these materials was witnessed after the theoretical prediction and experimental revelation that such compounds are superior three-dimensional (3D) topological insulators (TIs) [4, 5]. The crystals of Bi_2Q_3 have simple surface states in their bulk energy gaps, which are topologically protected. The spin states of surface electrons are coupled with momentum, which has a great potential for future spintronic applications. As the bulk energy gap of Bi_2Se_3 is as large as $\sim$0.3 eV, the crystal of Bi_2Se_3 is of particular interest for room temperature applications.

As-grown bulk crystals of Bi_2Se_3 usually show high concentrations of electrical carriers (electrons) and the Fermi levels are pinned to the conduction band [5, 6]. This hinders easy access to the TI states of the material. One may reduce the level of background doping by introducing acceptors in the crystal [7, 8]; however, such an approach is not appropriate when the background carrier density is high. A high density of dopants introduces scattering centers, which degrade the transport properties of the material. For quantum device applications, it is desirable to fabricate thin films or nanostructures of Bi_2Se_3. However, the situation is similar to bulk crystals in that background electron concentrations higher than $\sim 10^{19}$ cm^{-3} are consistently observed [9]–[13]. It is imperative to obtain high-quality films with low background doping for practical purposes. In this paper, we adopt the method of molecular beam epitaxy (MBE) operating in ultrahigh vacuum to grow Bi_2Se_3 layers on Si(111) substrate. Such a method was recently demonstrated to be successful for growing thin films of Bi_2Se_3 [14, 15] and Bi_2Te_3 [16]. Here, we investigate the van der Waals epitaxy (VdWe) method and report on the effectiveness of using a vicinal surface to achieve high-quality epitaxial layers.

The rhombohedral crystal of Bi_2Se_3 has a layered structure along the [111] crystallographic direction, where five atomic layers in the sequence -Se-Bi-Se-Bi-Se- form a quintuple layer (QL) unit. Atoms within the QL unit are chemically bonded, while between adjacent QLs, they are bonded by the weak van der Waals (vdW) force [17]. Such a unique structure of Bi_2Se_3 favors two-dimensional (2D) growth along the [111] direction using the so-called vdWe method [18]–[21]. The essence of vdWe is to prepare a substrate surface that does not contain dangling bonds. For Si(111)-(7 $\times$ 7) that is used in this study, surface dangling bonds do exist. We may saturate such dangling bonds by hydrogen atoms before Bi_2Se_3 deposition in order to achieve the vdWe mode [22], but here we introduce another approach in which the surface effect of the substrate can be suppressed using a two-step procedure. The initial deposition of a thin amorphous seed layer of Bi_2Se_3 at low temperature (LT) is followed by high-temperature

(HT) growth, and the later stage HT deposition on the seed layer proceeds via the vdWe mode. We will show that such a two-step approach has resulted in films that are superior to those grown using a single step process. To minimize in-plane twinning of the film, we employ the vicinal substrate surface (denoted as v-Si(111) hereafter). By optimizing the growth parameters (temperature and flux), Bi_2Se_3 thin films with an LT resistivity of $\sim 1\,m\Omega\,cm$, a carrier mobility of $\sim 2000\,cm^2\,V^{-1}\,s^{-1}$ and a carrier concentration of $\sim 3 \times 10^{18}\,cm^{-3}$ are obtained. The samples also show a relatively high and linearly dependent magnetoresistance (MR).

2. Experimental

Sample preparation and surface morphology measurements using scanning tunneling microscopy (STM) were carried out in a multi-chamber ultrahigh vacuum system, where the base pressure in the vacuum chambers was below 2×10^{-10} mbar. Atomic fluxes of Bi and Se were provided by standard K-cells, which were calibrated by an ion-gauge-based beam-flux monitor (BFM). Nominal flat Si(111) and vicinal (3.5° offcut from the (111) to $[\bar{1}\bar{1}2]$ direction) substrates were chemically cleaned and degassed overnight in vacuum before deoxidization at 1400 K to obtain the (7×7) reconstruction. Then, the surface was exposed to a flux of Bi until the Bi-induced β-phase $(\sqrt{3} \times \sqrt{3})$ structure was obtained. Bi_2Se_3 deposition was then initiated at ~ 100 K as cooled by liquid nitrogen. After the deposition of a few QLs, the temperature of the substrate was increased using radiation from a set of tungsten filaments. The temperature was monitored by a thermocouple near the sample stage, which had been calibrated *a priori* by the melting points of indium (443 K), selenium (493 K) and bismuth (543 K). The reflection high-energy electron diffraction (RHEED) patterns and the evolution of its intensity (I) and inter-streak spacing (D) were recorded by a charge-coupled device camera. For room-temperature STM measurements, the tunneling current was 0.2 nA and the sample bias was +0.8 V throughout. *Ex situ* x-ray diffraction (XRD) measurements were made on a high-resolution diffractometer from Bruker by using a Cu-Kα1 x-ray source. The temperature-dependent Hall and MR measurements were made in a Quantum Design PPMS system using the Hall bar devices. The Hall bars were fabricated by the standard photolithography technique with Cr(10 nm)/Au(150 nm) metal contacts deposited by thermal evaporation. Cross-section transmission electron microscopy (TEM) examination was carried out in a JEOL 2010F high-resolution transmission electron microscope working at 200 kV, and the TEM specimen was prepared by a standard procedure for mechanical thinning followed by Ar ion milling.

3. Growth of Bi_2Se_3 thin films

Prior to the LT deposition of Bi_2Se_3, the Si(111)-(7×7) substrate surface is exposed to a flux of Bi, achieving the β-phase $(\sqrt{3} \times \sqrt{3})$ structure of the substrate [23]. Then Bi_2Se_3 deposition is initiated at ~ 100 K using a high Se/Bi flux ratio of Se : Bi = 10 : 1. The growth front is monitored by RHEED. Figure 1(a_i) shows the evolution of the RHEED intensity I and the reciprocal lattice parameter D as the deposition proceeded. The lower panel shows a schematic illustration of the temperature change of the sample during deposition. The RHEED patterns taken along the $[1\bar{1}0]$ direction (the Miller indices are based on cubic Si throughout) at different growth stages are also given in figures 1(a_ii)–(a_iv). As can be seen, upon Bi_2Se_3 deposition at LT, a film with the same lattice constant as that of Bi_2Se_3 is immediately formed. After the growth of 1–2 QLs, the RHEED pattern disappears, indicating a fully disordered

or amorphous film. The RHEED intensity correspondingly drops and the lattice parameter becomes immeasurable. We let the growth continue for a further 2–3 QLs before gradually increasing the temperature to 520 K, at which a diffraction pattern characteristic of the Bi_2Se_3 crystal reappears suddenly at a total deposition coverage of ∼7 QLs. The reciprocal lattice parameter (D) also recovers instantaneously to that of Bi_2Se_3, suggesting a crystal Bi_2Se_3 layer formation. From the RHEED pattern of figure 1(a_ii), however, we note that the initial crystalline Bi_2Se_3 is textured, containing in-plane rotation domains in all directions. We then slightly lower the substrate temperature to 450 K for continuous growth of Bi_2Se_3. At this stage, the RHEED intensity starts to oscillate, suggesting the layer-by-layer growth mode. By comparing the oscillation period with the film thickness, we establish that one period of the RHEED oscillation corresponds to one QL deposition. Notably, after the growth of 2 QLs, the RHEED pattern becomes very clean, characteristic of single crystalline Bi_2Se_3. Although a weak 3D feature is also noted in the RHEED at this oscillation stage, the 3D feature gradually disappears as the growth continues. The improvement of the surface quality with film thickness is apparent from the RHEED evolution. The diffraction streaks become increasingly sharper while the background intensity weakens. Cross-sectional TEM study of a sample prepared by such a two-step method (figure 1(c)) shows that the initial amorphous seed layer remains during the subsequent HT growth stage. Therefore, the crystalline Bi_2Se_3 formed at the later HT growth stage is by a self-crystallization or organization process, without much influence from the substrate. The growth proceeds via vdWe. Figure 2(a) shows a large area STM image of the surface of a 200 nm-thick Bi_2Se_3 film. The surface is seen to consist of triangular step-and-terrace features, underlying an anisotropic lateral growth rate in different azimuthal directions. With reference to the lattices of the substrate, we establish that it grows at a faster rate in the $[\bar{1}\bar{1}2]$ direction than along $[11\bar{2}]$. The steps on the surface are 9.5 Å high, corresponding to one QL of Bi_2Se_3. The surface roughness is about 1.75 nm measured over an area of $2.5 \times 2.5\ \mu m^{-2}$, which is quite smooth considering the inherent step-height of 0.95 nm of the material. From the figure, one also observes oppositely orientated triangles with approximately equal proportion on the surface, indicating that the film contains twin defects. Twin boundaries are inevitable, one of which is revealed in the zoom-in STM image as shown in the inset of figure 2(a). Moreover, from STM measurements, we also observe step-terminations and spiral mounds that are associated with threading screw dislocations. One such dislocation is indicated by the dashed arrow in the inset of figure 2(a), and the density of such threading screws is estimated to be of the order of $\sim 10^9\ cm^{-2}$. Despite all the defects, such a film grown by the two-step method is still superior to the ones grown using a single step method. If Bi_2Se_3 is grown continuously at LT, a disordered or an amorphous-like film is obtained. Post-growth annealing may lead to crystallization of such films, but it can hardly result in high-quality crystals. On the other hand, if Bi_2Se_3 is grown at HT continuously from the beginning, layer-by-layer growth is indeed observable as judged from the RHEED intensity oscillations, but it is usually accompanied by some 3D features on the growth front. The surface smoothness, domain size and crystallinity are inferior to that grown using the two-step approach. For example, figure 1(a_v) shows a RHEED pattern of the HT-grown Bi_2Se_3 surface, revealing spotty and split diffraction patterns characteristic of the single step grown surfaces.

The existence of twins, even in films grown by the two-step method, is undesirable. Noting that the lateral growth rate is anisotropic, we resort to a vicinal substrate to bias the growth of one domain over the other [24, 25]. Using the same two-step approach but on v-Si(111), the evolution of the RHEED intensity, the reciprocal lattice parameter and the

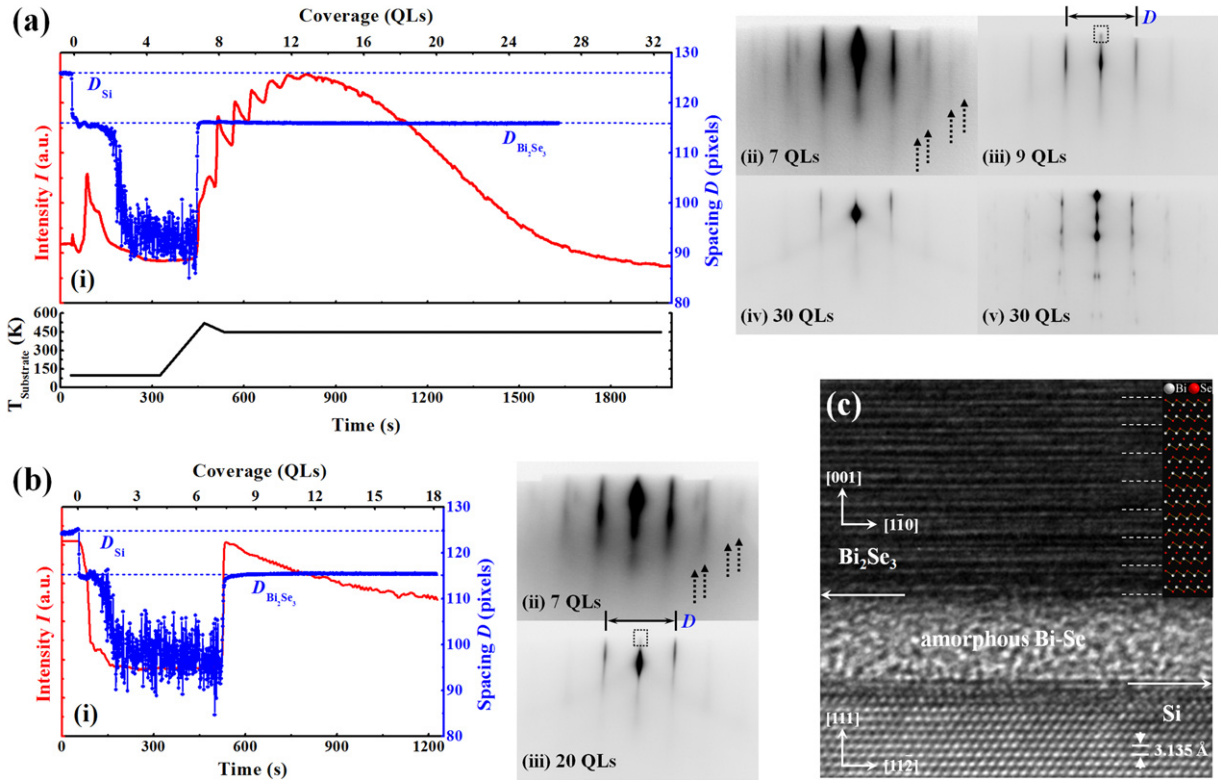

Figure 1. Evolution of the RHEED during Bi_2Se_3 deposition. In (a) and (b) are shown the RHEED observations during deposition on nominal flat and vicinal Si(111) surfaces, respectively. In (i), the evolution of the RHEED intensity (I, red curve) and spacing (D, blue curve) between two integer diffraction streaks, as a function of deposition time or coverage, is presented. In (a_ii)–(a_iv) and (b_ii)–(b_iii), the corresponding RHEED patterns from the growing surfaces at different growth stages are shown. In (a_v), the RHEED pattern of a surface prepared using a single step growth procedure is shown. In (a_ii) and (b_ii), the dashed arrows point to diffraction features originating from in-plane texture of the film, which are observable after annealing the LT-grown seed layer. The dashed squares in (a_iii) and (b_iii) mark the location from where the RHEED intensity I is measured (note that this location corresponds to an off-specular position but to a transmission diffraction spot of the bulk crystal; refer to (a_v)). In (a_i) and (b_i), two horizontal dotted lines show the expected D values of Si and Bi_2Se_3 crystals, respectively. The RHEED patterns shown in both (a_ii) and (b_ii) have been logarithmly treated to enhance the weak diffraction features. The panel below (a_i) illustrates the heating scheme of the sample during film deposition. (c) Cross-section TEM micrograph showing the amorphous seed layer between the Si substrate and epitaxial Bi_2Se_3. The dashed lines mark the gaps between adjacent QLs of Bi_2Se_3 and the inset shows a schematic drawing of the layered structure of the Bi_2Se_3 crystal.

RHEED patterns are given in figure 1(b). For the LT seed layer growth, a similar observation to that of the flat film growth was made. However, upon increasing the temperature for subsequent crystalline film formation, no RHEED intensity oscillation is recorded, suggesting the step-flow

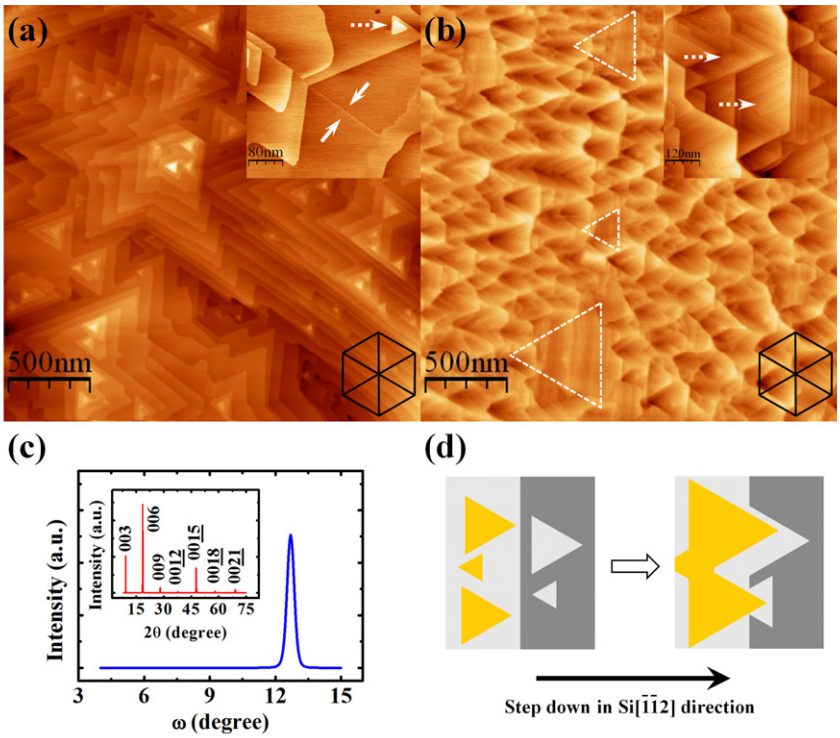

Figure 2. STM images of the surfaces of 200 nm thick epitaxial Bi_2Se_3 films and the x-ray data. (a) A large area STM image (size: $2.5 \times 2.5\,\mu m^2$) of the film surface grown on flat Si(111) substrate. The inset shows a close-up image (size: $400 \times 400\,nm^2$) of the same surface showing the boundary (pointed by solid arrows) between two 180° twins, and a spiral mound (pointed by the dashed arrow) at a threading screw dislocation. (b) A large area STM image (size: $2.5 \times 2.5\,\mu m^2$) of the film grown on vicinal Si(111) substrate. The dashed triangles mark a few twin defects in the film. The inset shows a zoom-in image (size: $600 \times 600\,nm^2$) of the surface, revealing threading dislocations near the domain boundaries (dashed arrows). The hexagons drawn at the bottom right of the main images indicate the crystallographic direction of the surface lattice, and it is along the $[\bar{1}\bar{1}2]$ direction from left to right. (c) XRD rocking curve of a vicinal Bi_2Se_3 film and the inset shows the reflective θ–2θ scan of the same sample. (d) Schematic illustration of the unbalanced growth of twin domains due to surface steps descending towards $[\bar{1}\bar{1}2]$. The gray, white and yellow colors mark terraces of different levels. Aggregation of islands by deposition causes the latter to coalesce with steps.

growth mode, possibly related to the presence of a high density of steps on the surface due to the vicinal substrate. Unlike that on the flat substrate, no 3D feature is ever noted during the HT growth stage on v-Si(111). The sharpness of the RHEED streaks and also the observation of Kikuchi lines indicate that the film is of high structural quality.

The advantage of using v-Si(111) is more apparent when examining the morphology of the grown films. Figure 2(b) shows an STM image of the surface of a 200 nm thick film, which displays a unique pointed-step structure. The pointed, rather than straight, step edges conform

to the fast growth rate along $[\bar{1}\bar{1}2]$. The oppositely oriented twin domains would show relatively straight descending steps, whereas the ascending steps on the opposite side, if present, would be similarly pointed. Examples of the latter domain areas in figure 2(b) are marked by the dashed triangles pointing to the left. However, such domains are a minority in the matrix of the 'right-pointing' step domain; therefore they are effectively suppressed by using the vicinal substrate. This may be understood from the fact that lateral growth of such domains would be in the direction of ascending steps, which is arrested by step flows during material deposition. Figure 2(d) schematically illustrates the suppression of the left-pointing triangular islands due to surface steps, leading to an imbalance of growth between two oppositely oriented domains as manifested by the left- and right-pointing triangular islands. Meanwhile, threading screw dislocations, observable only near the twin boundaries as exemplified in the inset of figure 2(b), are diminished by using the vicinal substrate. An estimate of such threading defects from the STM measurements results in a value of $\sim 10^8\,\mathrm{cm}^{-2}$, which is an order of magnitude reduction over that of flat films. To characterize the phase purity and crystal quality of such vicinal films, XRD rocking curves are measured, an example of which is shown in figure 2(c). A peak at $\sim 12.71^\circ$ is observed, corresponding nicely to the (0 0 6) diffraction of a Bi_2Se_3 crystal by noting the $\sim 3.5^\circ$ offcut angle of the substrate with respect to the (111) plane (the theoretical Bragg angle is 9.32°). This observation shows that there is little tilting of the epifilm from that of the substrate surface. The reflective θ–2θ scans of the sample shown in the inset of figure 2(c) reveal diffraction peaks that are all indexable to a crystalline Bi_2Se_3. Such an vicinal film shows an rms surface roughness of ~ 2.01 nm over the area of $2.5 \times 2.5\,\mu\mathrm{m}^{-2}$, which is slightly larger than the flat film. This may reflect the fact that there is a slight step bunching of the vicinal film as seen in figure 2(b).

4. Hall and magneto-transport measurements of Bi_2Se_3 thin films

The improvement of the surface and structural quality of Bi_2Se_3 by using v-Si has also led to an improvement of the electronic properties of the films. Figure 3(a) compares the temperature dependence of the film's resistivity between a flat (i) and a vicinal (ii) film of the same thickness (200 nm). The two samples were grown at exactly the same MBE condition ($T = 450\,\mathrm{K}$, $\mathrm{Se} : \mathrm{Bi} = 10 : 1$) and using the same two-step growth procedure. Data measured at temperatures above 150 K contain contributions from the substrate due to ionization of phosphor dopant in Si and thus a decreased overall resistivity, so they are not shown here. It can be seen that the resistivity of Bi_2Se_3 on v-Si(111) is consistently higher than that on the flat substrate. Figure 3(b) shows temperature-dependent carrier densities and mobility in the same flat (i) and vicinal (ii) films, respectively. A background electron concentration of $\sim 3 \times 10^{19}\,\mathrm{cm}^{-3}$ is observed in the flat film, and the mobility is $\sim 1200\,\mathrm{cm}^2\,\mathrm{V}^{-1}\,\mathrm{s}^{-1}$ at 2 K. On the other hand, the vicinal film shows a carrier concentration of $\sim 5 \times 10^{18}\,\mathrm{cm}^{-3}$ and a mobility of $\sim 1600\,\mathrm{cm}^2\,\mathrm{V}^{-1}\,\mathrm{s}^{-1}$ at the same temperature. The best sample we have measured shows a background electron density of $3 \times 10^{18}\,\mathrm{cm}^{-3}$ and a mobility of $2000\,\mathrm{cm}^2\,\mathrm{V}^{-1}\,\mathrm{s}^{-1}$. Such a background carrier density represents an order of magnitude reduction over the best flat samples. As point defects are more likely related to growth conditions of the MBE (refer to figures 3(c) and (d)), such a reduction of background doping in vicinal films is likely linked to the reduction of extended defects, such as twin boundaries and dislocations, where Se vacancies created at such defects may act as donors of the films. The fact that the background carrier densities do not change much with temperature (figure 3(b)) indicates full ionization of electron donors in Bi_2Se_3 even at LT. On the other hand,

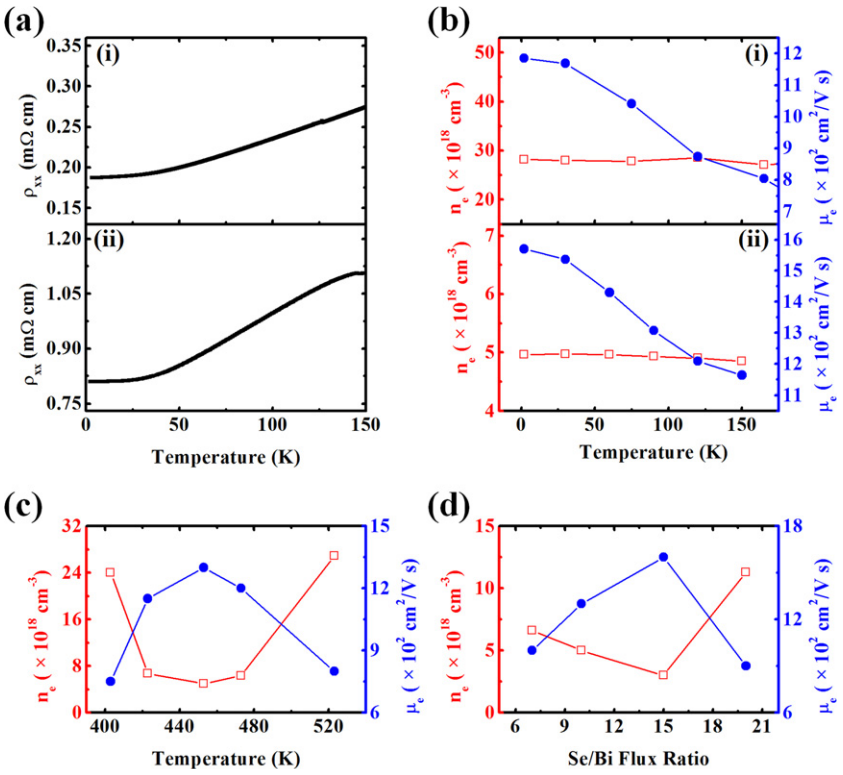

Figure 3. Resistivity and Hall density and mobility of as-grown Bi_2Se_3 films (200 nm thick). (a) Resistivity (ρ_{xx}) as a function of temperature of the as-grown Bi_2Se_3 film on (i) flat and (ii) vicinal Si(111) surfaces, respectively. (b) Hall density (n_e) and mobility (μ_e) of electrons in (i) flat and (ii) vicinal films. (c, d) Dependence of the background electron density (n_e, red squares) and mobility (μ_e, blue circles) on (c) deposition temperature and (d) the Se/Bi flux ratio of MBE. The data in (c) and (d) have been obtained by Hall measurements at $\sim$100 K.

increasing the temperature caused a notable decrease of electron mobility, implying phonon scattering processes. Finally, the MBE condition will affect point defect formation, causing additional modification of the electronic behavior of the films. Figures 3(c) and (d) show, respectively, the effects of both substrate temperature and Se-to-Bi flux ratio on the density and mobility of electrons in films. The samples appear superior when grown at temperatures in the range of 420–470 K (i.e. from $1/5T_m$ to $1/3.5T_m$, where $T_m \sim 710\,^{\circ}$C is the melting point of Bi_2Se_3) and at the flux ratio of 7:1–15:1. It is noted that under such growth conditions, the films also show good morphologies and structural quality. At too low a temperature, the crystallinity of the film degrades, as indicated by a high density of dislocations and twin boundaries, whereas growth at too high a temperature causes the surface to contain cracks and holes, probably due to material decomposition. Although higher Se-to-Bi flux ratios ($>20:1$) may consistently produce good surfaces of the epifilms, the electronic property degrades, probably due to the creation of anti-site or interstitial Se in the film. At low flux ratios ($<5:1$), other more Bi-rich phase(s) of Bi-Se may form in addition to Bi_2Se_3, as revealed by some preliminary XRD measurements.

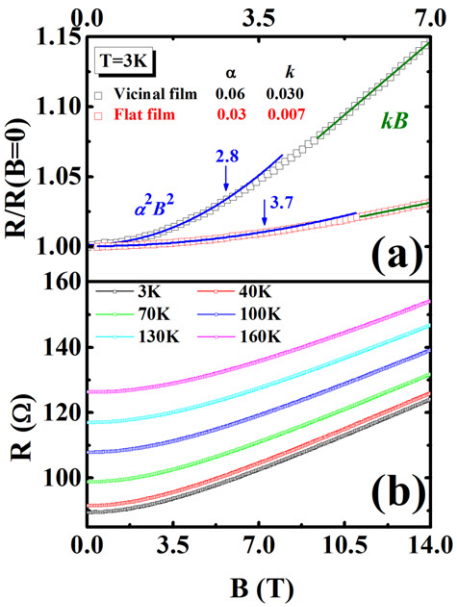

Figure 4. (a) MR of Bi_2Se_3 films (200 nm thick). (a) Normalized resistance $R/R(B=0)$ of flat and vicinal films as a function of perpendicular magnetic field at $T=3$ K. At low B field, the $R(B)$ curve shows a B^2 dependence, as shown by the solid blue fitting lines. At high B field, linear dependence of R on B is observed as shown by the solid green lines. The fitting parameters (α and k) are listed in the figure. The arrows points to the cutoff field. (b) $R(B)$ curves measured in the vicinal film at temperature ranging from 3 to 160 K and at B field up to 14 T. Linear B dependence at high magnetic field is clearly seen at each temperature.

Finally, the magneto-transport properties of flat and vicinal Bi_2Se_3 films were studied. Figure 4(a) shows the normalized MR $R/R(B=0)$ of flat (red circle) and vicinal (black square) Bi_2Se_3 films (200 nm thick) as a function of the perpendicular magnetic field (B) up to 7 T at $T=3$ K, respectively. One can see that the MR of both films at lower B field can be fitted well by a parabolic dependence: $R/R(B=0)=1+(\alpha\times B)^2$, as shown by the solid blue curves with the respective α values in figure 4(a). This dependence is believed to result from the Lorentz force deflection of carriers and α is proportional to the mobility [26]. As is apparent, the vicinal film shows a much larger MR than the flat one. We note that the electron mobility for the vicinal film ($\mu_{\text{vicinal}}\sim 1600\,\text{cm}^2\,\text{V}^{-1}\text{s}^{-1}$) is higher than that for the flat film ($\mu_{\text{flat}}\sim 1200\,\text{cm}^2\,\text{V}^{-1}\text{s}^{-1}$); (refer to figure 3(b)), which results in a higher α for the vicinal film ($\alpha_{\text{vicinal}}\sim 0.06$) than for the flat film ($\alpha_{\text{flat}}\sim 0.03$), and the $\mu_{\text{vicinal}}/\mu_{\text{flat}}$ ratio $\sim$1.3 is also in reasonable agreement with the $\alpha_{\text{vicinal}}/\alpha_{\text{flat}}$ ratio $\sim$2. However, a crossover from this parabolic dependence to a linear dependence of MR is observed at higher B field. The cutoff fields for the parabolic fits for both vicinal and flat films are indicated by arrows in figure 4(a). To help us see this crossover more clearly, figure 4(b) presents the MR of the vicinal film at B field up to 14 T. The linear dependence of MR at higher B field is clearly observed at all temperatures from 3 to 160 K. According to the theory of Abrikosov [27], a gapless semiconductor with linear dependence of energy on crystal momentum would exhibit a linear MR in the quantum

limit. This so-called 'quantum linear magnetoresistance' (QLMR) predicts that the linear slope is independent of temperature but is proportional to $1/n_e^2$. Indeed, $R(B)$ curves in figure 4(b) show almost identical linear slopes with the temperature ranging from 3 to 160 K. Furthermore, as shown in figure 4(a) (solid green lines), the MR of both the films at higher B field can be fitted well by a linear relationship $R/R(B=0) \propto kB$. The vicinal film shows a larger linear slope ($k_{\text{vicinal}} \sim 0.03$) than the flat one ($k_{\text{flat}} \sim 0.007$), reflecting that the carrier density of the vicinal film ($\sim 5 \times 10^{18}\,\text{cm}^{-3}$) is lower than that of the flat film ($\sim 3 \times 10^{19}\,\text{cm}^{-3}$). Therefore, we attempt to attribute the observed high-field linear MR to this QLMR, which could arise from the Dirac electrons of the topologically protected 2D surface states [4, 5]. The observation of QLMR as an indication of the existence of 2D topological surface states was also noted in a recent study on Bi_2Se_3 nanoribbons [28].

5. Conclusions

In summary, to minimize the effect of Si substrate lattice, a two-step growth procedure is adopted, where the LT amorphous seed layer of a few QLs thickness is kinetically stabilized on Si(111), whereas the amorphous seed layer serves as the 'substrate' for subsequent vdWe of crystalline Bi_2Se_3 at HT. By employing vicinal substrates, in-plane twinning of the epilayer is effectively suppressed due to directional flow of surface steps. By optimizing the growth conditions of MBE, crystalline Bi_2Se_3 thin films with an LT resistivity of $\sim 1\,\text{m}\Omega\,\text{cm}$, a carrier mobility of $\sim 2000\,\text{cm}^2\,\text{V}^{-1}\,\text{s}^{-1}$ and an electron density of $\sim 3 \times 10^{18}\,\text{cm}^{-3}$ are achieved. The epitaxial Bi_2Se_3 film shows a relatively high MR and a linearly dependent MR at high magnetic field, which are likely related to the topological surface states of the sample.

Acknowledgment

We are grateful to W K Ho for technical support in the growth experiments and to Stephen S Y Chui for assistance with XRD experiments. The PPMS facilities used for the magneto-transport measurements are supported by a Special Equipment Grant (SEG_CUHK06) from the University Grants Committee of Hong Kong Special Administrative Region (HKSAR). This work was financially supported by a Collaborative Research Fund from the Research Grant Council of HKSAR, China, under grant no. HKU 10/CRF/08, and by a Seed Fund for Basic Research from HKU.

References

[1] Wood C 1988 *Rep. Prog. Phys.* **51** 459
[2] Tritt T M 1999 *Science* **283** 804
[3] Venkatasubramanian R, Siivola E, Colpitts T and O'Quinn B 2001 *Nature* **413** 597
[4] Zhang H J, Liu C X, Qi X L, Dai X, Fang Z and Zhang S C 2009 *Nat. Phys.* **5** 438
[5] Xia Y *et al* 2009 *Nat. Phys.* **5** 398
[6] Chen Y L *et al* 2009 *Science* **325** 178
[7] Hor Y S, Richardella A, Roushan P, Xia Y, Checkelsky J G, Yazdani A, Hasan M Z, Ong N P and Cava R J 2009 *Phys. Rev.* B **79** 195208
[8] Checkelsky J G, Hor Y S, Liu M H, Qu D X, Cava R J and Ong N P 2009 *Phys. Rev. Lett.* **103** 246601
[9] Nataraj D, Senthil K, Narayandass S K and Mangalaraj D 1999 *Cryst. Res. Technol.* **34** 867

[10] Al Bayaz A, Giani A, Artaud M C, Foucaran A, Pascal-Delannoy F and Boyer A 2002 *J. Cryst. Growth* **241** 463
[11] Giani A, Al Bayaz A, Foucaran A, Pascal-Delannoy F and Boyer A 2002 *J. Cryst. Growth* **236** 217
[12] Fouad S S, Morsy A Y, Talaat H M and Eltawab M E 1994 *Phys. Status Solidi* b **183** 149
[13] Al Bayaz A, Giani A, Foucaran A, Pascal-Delannoy E and Boyer A 2003 *Thin Solid Films* **441** 1
[14] Zhang G H, Qin H J, Teng J, Guo J D, Guo Q L, Dai X, Fang Z and Wu K H 2009 *Appl. Phys. Lett.* **95** 053114
[15] Zhang Y *et al* 2010 *Nat. Phys.* **6** 584
[16] Li Y Y *et al* 2010 *Adv. Mater.* **22** 4002
[17] Lind H, Lidin S and Haussermann U 2005 *Phys. Rev.* B **72** 184101
[18] Koma A, Sunouchi K and Miyajima T 1985 *J. Vac. Sci. Technol.* B **3** 724
[19] Koma A 1992 *Thin Solid Films* **216** 72
[20] Koma A 1992 *Surf. Sci.* **267** 29
[21] Koma A 1999 *J. Cryst. Growth* **201** 236
[22] Liu K Y, Ueno K, Fujikawa Y, Saiki K and Koma A 1993 *Japan. J. Appl. Phys.* 2 **32** L434
[23] Wan K J, Guo T, Ford W K and Hermanson J C 1991 *Phys. Rev.* B **44** 3471
[24] Xie M H, Zheng L X, Cheung S H, Ng Y F, Wu H S, Tong S Y and Ohtani N 2000 *Appl. Phys. Lett.* **77** 1105
[25] Huang X R, Bai J, Dudley M, Wagner B, Davis R F and Zhu Y 2005 *Phys. Rev. Lett.* **95** 086101
[26] Smith R A 1978 *Semiconductors* (Cambridge: Cambridge University Press)
[27] Abrikosov A A 2000 *Europhys. Lett.* **49** 789
[28] Tang H, Liang D, Qiu Richard L J and Gao Xuan P A 2010 Magneto-transport effects in topological insulator Bi_2Se_3 nanoribbons arXiv:1003.6099v4